IEEE Access
Multidisciplinary ⋮ Rapid Review ⋮ Open Access Journal

Received November 2, 2019, accepted November 18, 2019, date of publication November 29, 2019, date of current version December 31, 2019.

Digital Object Identifier 10.1109/ACCESS.2019.2956837

Tight Coupling Dual-Band Coupler With Large Frequency Ratio and Arbitrary Power Division Ratios Over Two Bands

LIANG GAO[1], SHAO YONG ZHENG[1], (Senior Member, IEEE), WONBIN HONG[2], (Senior Member, IEEE), AND YUANXIN LI[1], (Member, IEEE)
[1]School of Electronics and Information Technology, Sun Yat-sen University, Guangzhou 510006, China
[2]Department of Electrical Engineering, Pohang University of Science and Technology, Pohang 37673, South Korea

Corresponding author: Shao Yong Zheng (zhengshaoy@mail.sysu.edu.cn)

This work was supported by the National Natural Science Foundation of China under Grant 61671485.

ABSTRACT To satisfy the requirements of the emerging wireless communication system, the simultaneous implementation of large frequency ratio and tight coupling is demanded for a dual-band coupler. But most of the existing dual-band coupler structures can only achieve one of them. In this paper, a new coupled line based dual-band coupler structure is proposed. The detailed theoretical analysis is conducted for different ranges of frequency ratio. It was shown that a wide frequency ratio from 1.4 to 11.7 can be achieved even for the designs which require a tight coupling of 3 dB. For higher flexibility, the same circuit topology is further investigated to implement the arbitrary power division ratios over the two bands. More importantly, the design parameters for the large frequency ratio and arbitrary power division ratio are found to be almost independent resulting in a simple design procedure. For demonstration purposes, a dual-band 3 dB coupler with a large frequency ratio of 6 is designed, fabricated and measured. Furthermore, another dual-band coupler with coupling coefficients of 3 dB and 6 dB at 2 GHz and 4 GHz is designed, fabricated and measured. Good agreement between simulation and measurement can be observed for both prototypes.

INDEX TERMS Dual-band coupler, coupled-line coupler, large frequency ratio, arbitrary power division ratio, tight coupling.

I. INTRODUCTION

With rapid development of wireless communications, different standards have emerged for various applications. In order to support different standards in a compact system, the components of the system are required to operate at two/multiple frequencies simultaneously. Among the components, the coupler is considered to be one of the most important ones, as it provides the signals with the desired amplitude and phase characteristics for the next component. Therefore, a lot of efforts have been made by the researchers to implement different types of dual-band couplers.

For a planar quadrature coupler, it is usually constructed using three basic topologies: branch line, patch element, and coupled line. To implement dual-band operation on a branch line based coupler, the most common approach is replacing the single-band transmission line with the equivalent dual-band transmission line. The dual-band transmission lines could be realized by using composite left-/right- hand transmission lines [1] and stub loaded transmission lines [2]–[4]. Considering the coupling effects between branches [5], [6] or adding cross coupled branches [7], dual-band operation could also be realized. The port extension approach [8], [9] is also an alternative for dual-band operation. Since the operating principle of a patch coupler is different from that of a branch line based structure, different approaches are required. Open stubs [10] and complementary split ring resonators (CSRR) [11] can be loaded onto a single band patch coupler to realize dual-band operation. For the coupled line based coupler, the coupled open stubs were added to the coupled-line section to realize dual-band operation [12].

To satisfy the various requirements for different application scenarios, further improvements on these dual-band couplers have been reported. For example, the size reduction utilizing stepped impedance stubs [13], arbitrary power division

The associate editor coordinating the review of this manuscript and approving it for publication was Feng Lin.

This work is licensed under a Creative Commons Attribution 4.0 License. For more information, see http://creativecommons.org/licenses/by/4.0/

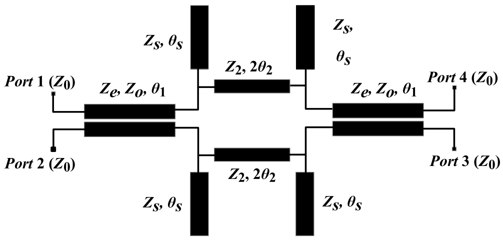

FIGURE 1. Schematic of the proposed coupled-line coupler.

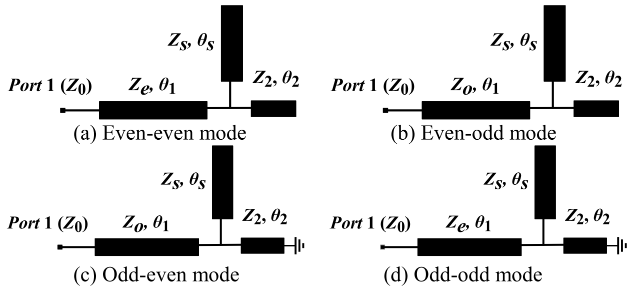

FIGURE 2. The sub circuits of the proposed coupler under the even and odd symmetric excitations.

ratio [14] and phase difference [15] were implemented in two bands. For most of the branch line based dual-band couplers, the frequency ratio is usually lower than 3. This is not sufficient to support the most popular existing standards within a single system. To solve this problem, three different configurations were proposed [16] which achieved the largest frequency ratios of 7, 10 and 5.4 respectively. But The configurations with a larger frequency ratio could only provide weak coupling. In [17], the frequency ratio and bandwidth were further extended based on the configuration proposed in [16]. It was based on a cascading method but again only possible for weak coupling. Since the equal power division is an important characteristic of a coupler, the applications of the existing coupler configurations with large frequency ratio are limited. In addition, arbitrary power division ratios over two bands is also important for a coupler with a large frequency ratio, which has not previously been realized. To solve this problem, the aperture coupling mechanism was proposed to feed two elements simultaneously to implement a dual-band coupler which can achieve a large frequency ratio up to 33.3 [18]. However, this structure is more suitable for the applications in which the higher frequency is within the millimeter wave frequency band, as the SIW element becomes bulky when the operating frequency is within the microwave frequency band. Therefore, a new structure that can achieve a large frequency ratio, tight coupling, and arbitrary power division ratios over the two bands is required.

II. THEORETICAL ANALYSIS

The schematic of the proposed dual-band coupled-line coupler is shown in Fig. 1. The circuit consists of two sections of coupled line and two interconnected transmission lines with end-loaded open stubs. The coupled lines have even- and odd-mode impedances of Z_e and Z_o and the electrical length of θ_1. The characteristic impedance and electrical length of the transmission lines that connect them are Z_2 and θ_2 respectively. For the open stubs, the corresponding parameters are Z_s and θ_s. The port impedance is set to Z_0. The even-odd mode approach is applied to analyze this circuit. The corresponding sub-circuits under different excitation conditions are shown in Fig. 2.

The scattering parameters of the proposed structure can be expressed by using the reflection coefficients of the even–even-, even–odd-, odd–even-, odd–odd- mode equivalent sub-circuits as follows.

$$S_{11} = \frac{(\Gamma_{ee}+\Gamma_{eo})+(\Gamma_{oe}+\Gamma_{oo})}{4} \tag{1a}$$
$$S_{21} = \frac{(\Gamma_{ee}+\Gamma_{eo})-(\Gamma_{oe}+\Gamma_{oo})}{4} \tag{1b}$$
$$S_{31} = \frac{(\Gamma_{ee}-\Gamma_{eo})-(\Gamma_{oe}-\Gamma_{oo})}{4} \tag{1c}$$
$$S_{41} = \frac{(\Gamma_{ee}-\Gamma_{eo})+(\Gamma_{oe}-\Gamma_{oo})}{4} \tag{1d}$$

For simplification, all characteristic impedance values are normalized to the port impedance Z_0 as follows.

$$z_e = \frac{Z_e}{Z_0},\quad z_o = \frac{Z_o}{Z_0},\ z_2 = \frac{Z_2}{Z_0},\ z_s = \frac{Z_s}{Z_0} \tag{2}$$

For the sub-circuits, the corresponding reflection coefficients can be calculated as

$$\Gamma_{ee} = \frac{z_{ee}-1}{z_{ee}+1} \tag{3a}$$
$$\Gamma_{eo} = \frac{z_{eo}-1}{z_{eo}+1} \tag{3b}$$
$$\Gamma_{oe} = \frac{z_{oe}-1}{z_{oe}+1} \tag{3c}$$
$$\Gamma_{oo} = \frac{z_{oo}-1}{z_{oo}+1} \tag{3d}$$

where

$$z_{ee} = \frac{z_e\left(z_2 z_s + j z_e \tan(\theta_1)\left(z_2 + j z_s \tan(\theta_2)\right)\right)}{z_e z_2 + j z_s\left(z_2 \tan(\theta_1) + z_e \tan(\theta_2)\right)} \tag{4a}$$
$$z_{eo} = \frac{z_e\left(z_2 z_s + z_e\left(j z_2 + z_s \cot(\theta_2)\right)\tan(\theta_1)\right)}{-j z_e z_s \cot(\theta_2) + z_2\left(z_e + j z_s \tan(\theta_1)\right)} \tag{4b}$$
$$z_{oe} = \frac{z_o\left(z_2 z_s + j z_o \tan(\theta_1)\left(z_2 + j z_s \tan(\theta_2)\right)\right)}{z_o z_2 + j z_s\left(z_2 \tan(\theta_1) + z_o \tan(\theta_2)\right)} \tag{4c}$$
$$z_{oo} = \frac{z_o\left(z_2 z_s + z_o\left(j z_2 + z_s \cot(\theta_2)\right)\tan(\theta_1)\right)}{-j z_o z_s \cot(\theta_2) + z_2\left(z_o + j z_s \tan(\theta_1)\right)} \tag{4d}$$

The conditions for perfect input matching ($S_{11} = 0$) and isolation ($S_{31} = 0$) lead to the following relationships.

$$\Gamma_{ee} + \Gamma_{oo} = 0 \tag{5a}$$
$$\Gamma_{eo} + \Gamma_{oe} = 0 \tag{5b}$$

Combing (3) and (4) we obtain

$$z_{ee} z_{oo} = z_{eo} z_{oe} = 1 \tag{6}$$

Substituting (4) into (5) gives the following matching and isolation conditions.

$$z_e z_o = 1 \quad (7a)$$

$$z_s^2\left(1 - z_2^2\right)\cot(\theta_s)^2 + 2z_s z_2\cot(2\theta_2)\cot(\theta_s) - z_2^2 = 0 \quad (7b)$$

Since the coupler is designed to provide arbitrary power division at output ports with a 90° phase difference, the relationship between the coupling and transmission parameters should be

$$S_{41} = jkS_{21} \quad (8)$$

where k is the power-dividing coefficient. By combing (1), (3), and (7), the following equation can be obtained.

$$kj(z_{ee}z_{eo} - 1) = z_{ee} - z_{eo} \quad (9)$$

Substituting (4) into (9) yields the following equation.

$$k = \frac{-\left(z_2 z_e^2 z_s^2\cot(\theta_s)^2\csc(\theta_2)^2\sec(\theta_1)^2\right)}{A - B + C} \quad (10)$$

where A, B, C are given in (14), as shown at the bottom of the next page. Equations (7) and (10) are the key formulas in designing the desired dual-band couplers. Equations (7b) and (10) can be expressed by the following general equations.

$$f_1(z_2, z_s, \theta_2, \theta_s) = 0 \quad (11a)$$

$$f_2(z_e, z_2, z_s, \theta_1, \theta_2, \theta_s) = k \quad (11b)$$

If θ_2 is determined as the reference electrical length at f_L, θ_1 and θ_s are denoted by $r_1\theta_2$ and $r_2\theta_2 (r_1, r_2 = 1, 2, 3\ldots)$.

III. TIGHT COUPLING DUAL BAND COUPLER WITH WIDE FREQUENCY RATIO

A. Case I ($\theta_1 = 4\theta_2, \theta_s = 2\theta_2$, FR: 2.3-4.4)

For the case of $r_1 = 4, r_2 = 2, 4\theta_2$ and $2\theta_2$ are used to replace θ_1 and θ_s in (7b) and (10) respectively. Then it can be found that two equations remain equal if θ_2 is replaced by $n_1\pi/2 - \theta_2$ ($n_1 = 1, 2, 3\ldots$). If θ_2 corresponds to the low frequency f_L, $n_1\pi/2 - \theta_2$ is the electrical length at high frequency f_H. The phase difference between S_{41} and S_{21} equals to 90° at the two frequencies, as (11b) remains the same for the two frequencies. Thus, the frequency ratio FR can be expressed as $f_H/f_L = (n_1\pi/2 - \theta_2)/\theta_2$. For a compact size, n_1 is set to 1. The electrical lengths of the dual-band coupler at f_L can be found in the following.

$$\theta_2 = \frac{1}{1+\frac{f_H}{f_L}}\frac{\pi}{2} = \frac{\pi/2}{1+FR} \quad (12a)$$

$$\theta_1 = r_1\theta_2 = \frac{2\pi}{1+FR} \quad (12b)$$

$$\theta_s = r_2\theta_2 = \frac{\pi}{1+FR} \quad (12c)$$

Consequently, (11) can be expressed as

$$f_1(z_2, z_s, FR) = 0 \quad (13a)$$

$$f_2(z_e, z_2, z_s, FR) = k \quad (13b)$$

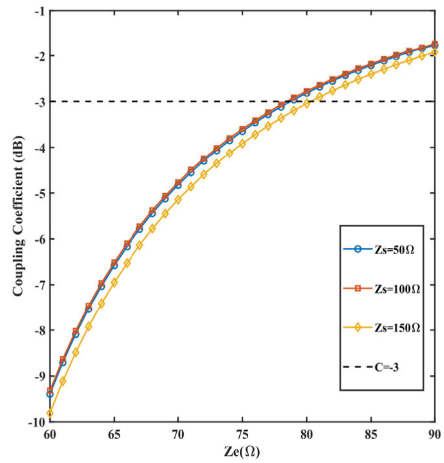

FIGURE 3. Coupling coefficient versus even-mode impedance of coupled-line sections with various Z_s values. $C = 10\,log_{10}(1/(1+k^2))$.

It can be found from (13a) that the frequency ratio FR is mainly determined by the values of Z_2 and Z_s. Once the FR is determined, there are an infinite number of solutions for Z_2 and Z_s. From (13b), k is found to be determined by Z_e, Z_2, and Z_s for a given FR. According to the investigation on this equation, it can be observed that Z_e plays the most important role in determining the coupling coefficient. From (13a) and (13b), by eliminating Z_2 and setting FR to 3, the curves of the coupling coefficient (C) versus Z_e with various Z_s can be plotted, as shown in Fig. 3.

From Fig. 3, most of the curves are found to follow closely with each other for various values of Z_s, thus Z_e can effectively be used to control the coupling coefficient. It can be concluded that Z_2 and Z_s can be used to determine the FR while Z_e can be used to control the coupling coefficient. That means the design of frequency ratio and power division ratio can be treated independently. Thus, the proposed coupler is simple to design and its performance is almost independent of frequency ratio. Once the desired coupling coefficient is set, the approximate range of Z_e can be determined accordingly by using Fig. 3. For example, if a coupling coefficient C of -3 dB is desired, an approximate value of Z_e from 78 to 86 (the corresponding Z_e/Z_o is from 2.43 to 3) can be chosen according to Fig. 3. In fact, for a realizable frequency ratio, Z_e is always within the realizable range of a coupled line.

To implement a dual-band coupler with tight coupling, Z_e is set to 80 Ohm based on the above analysis. With Z_e determined, four variables (Z_2, Z_s, FR, and k) and equations (13a, b), the relationship between Z_2, Z_s and k can be plotted in a contour map by eliminating FR. This is shown in Fig. 4 using the dashed lines. The numbers labeled on the dashed line is the power dividing coefficient. As a tight coupling is desired, only the contour line with k varying from 0.95 to 1.1 is shown plotted. At the same time, equation (13a) can be used to plot a contour map in the same figure, as shown by the solid line in Fig. 4. The numbers labeled on the solid line is the frequency ratio. It should be

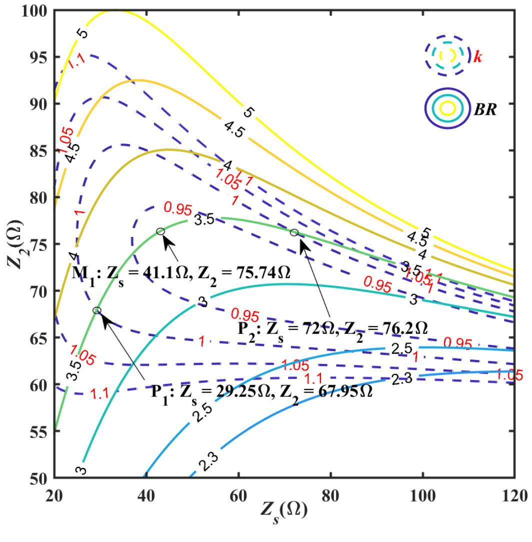

FIGURE 4. Contour map for k and FR versus Z_s and Z_2 for Case I.

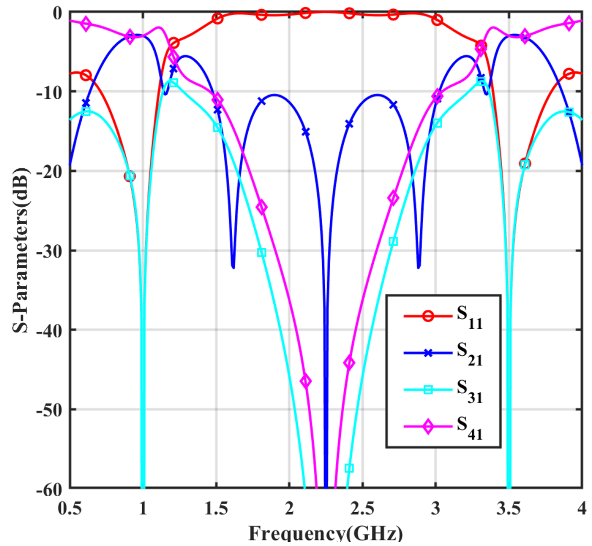

FIGURE 5. Calculated S-parameters of the design corresponding to the point P_1 in Fig. 4.

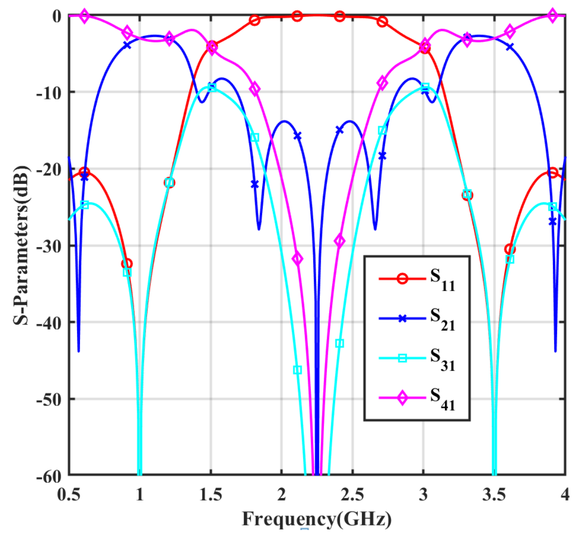

FIGURE 6. Calculated S-parameters of the design corresponding to the point P_2 in Fig. 4.

mentioned that if different coupling coefficients are needed, the corresponding Z_e can be chosen according to Fig. 3, and the contour map can then be plotted to obtain the design parameters.

Fig. 4 provides useful information for the design of Case I couplers. Firstly, k remains in the range of tight coupling for different FR for the same Z_e. This verifies the statement given above, that is, Z_e is mainly responsible for controlling the coupling coefficient. Secondly, the realizable FR range can be determined. In the area of tight coupling (the dashed line covered area), the FR ranges from 2.3 to 5. Finally, this figure can be used to design Case I couplers easily. For instance, if a dual-band coupler with a FR of 3.5 is desired, there are two solutions as there are two intersection points (P_1 and P_2) in the contour lines for $FR = 3.5$ and $k = 1$. If the low frequency center point f_L is set to be 1 GHz, and the corresponding high frequency center point is 3.5 GHz. The electrical lengths of θ_1, θ_2, θ_s can be calculated as 80°, 20°, 40° by using (12). Z_e is predetermined to be 80 Ω. At the point P_1, Z_s and Z_2 are determined as 29.25 Ω and 67.95 Ω respectively. At the point P_2, Z_s and Z_2 are determined as 72 Ω and 76.2 Ω respectively. Figs. 5 and 6 show the calculated S-parameters of the two designs which correspond to the points P_1 and P_2. It can be found that these two designs both exhibit a narrow bandwidth.

Thus the middle point M_1 between these two points is chosen alternatively. At the point M_1, Z_s and Z_2 are determined as 41.1 Ω and 75.74 Ω respectively. The corresponding calculated S-parameters are shown in Fig. 7. As expected, a wider bandwidth is achieved.

B. Case II ($\theta_1 = 6\theta_2, \theta_s = 2\theta_2$, FR: 3.8-7)

Similar to Case I, $6\theta_2$ and $2\theta_2$ are used to replace θ_1 and θ_s in (7b) and (10) respectively. Two equations still remain equal if θ_2 is replaced by $n_1\pi/2 - \theta_2 (n_1 = 1, 2, 3\ldots)$.

$$\begin{aligned}
A &= z_e^2(z_2^2\cot(\theta_2) - z_2 z_s\left(-1+\cot(\theta_2)^2\right)\cot(\theta_s) + \left(-1+z_2^2\right) z_s^2\cot(\theta_2)\cot(\theta_s)^2) \\
B &= z_2 z_e\left(-1+z_e^2\right) z_s\cot(\theta_s)\left(2z_2\cot(\theta_2) - z_s\left(-1+\cot(\theta_2)^2\right)\cot(\theta_s)\right)\tan(\theta_1) \\
C &= \left(z_2^2 z_e^4\cot(\theta_2) - z_2 z_e^4 z_s\left(-1+\cot(\theta_2)^2\right)\cot(\theta_s) + \left(z_2^2 - z_e^4\right) z_s^2\cot(\theta_2)\cot(\theta_s)^2\right)\tan(\theta_1)^2
\end{aligned} \tag{14}$$

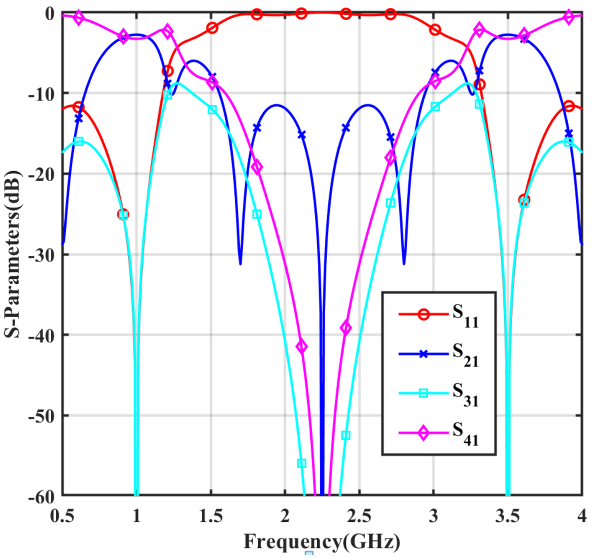

FIGURE 7. Calculated S-parameters of the design corresponding to the point M_1 in Fig. 4.

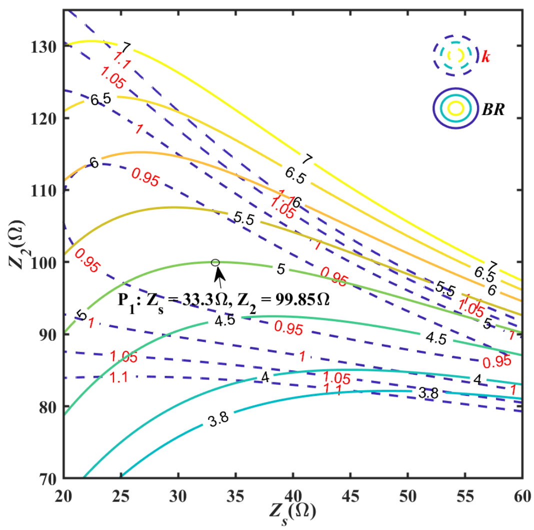

FIGURE 8. Contour map for k and FR versus Z_s and Z_2 for Case II.

n_1 is set to 1 for compactness. If θ_2 corresponds to the low frequency f_L, $\pi/2 - \theta_2$ is the electrical length at high frequency f_H. At the two operating frequencies, the phase difference between S_{41} and S_{21} equals to 90° and the related parameters of the Case II coupler at f_L still can be obtained as $\theta_2 = (\pi/2)/(1+FR), \theta_1 = 3\pi/(1+FR)$, $\theta_s = \pi/(1+FR)$.

Fig. 8 shows the contour map for designing the Case II coupler. From the figure, it can be seen that the realizable FR range for Case II is found to range from 3.8 to 7. As an example, for a tight coupling dual-band coupler with a FR of 5, the point P_1 is chosen in Fig. 8. The electrical lengths of θ_1, θ_2, θ_s can be calculated as 90°, 15°, 30°. Z_e is predetermined to be 80 Ω. Z_s and Z_2 are determined as 33.3 Ω and 99.85 Ω

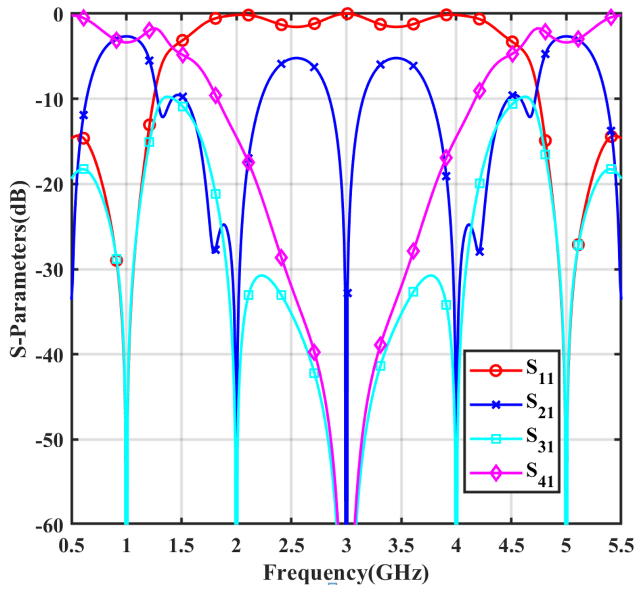

FIGURE 9. Calculated S-parameters of the design corresponding to the point P_1 in Fig. 8.

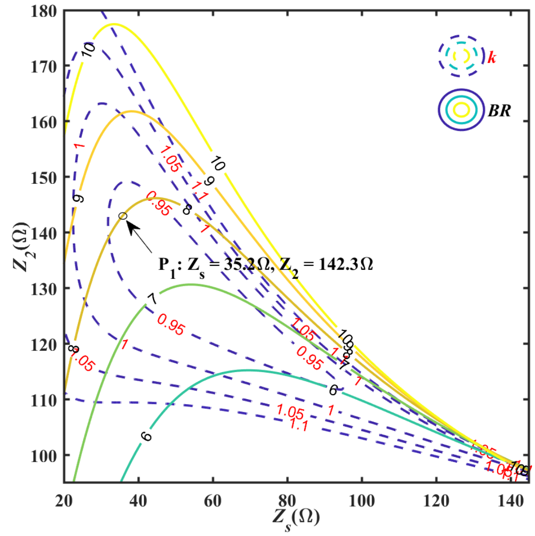

FIGURE 10. Contour map for k and FR versus Z_s and Z_2 for Case III.

respectively. The calculated S-parameters of the design which corresponds to point P_1 are shown in Fig. 9.

C. Case III ($\theta_1 = 8\theta_2, \theta_s = 4\theta_2$, FR: 6 -9.4)

For Case III, $8\theta_2$ and $4\theta_2$ are used to replace θ_1 and θ_s in (7b) and in (10). The related parameters of this coupler at f_L can be obtain as: $\theta_2 = (\pi/2)/(1+FR), \theta_1 = 4\pi/(1+FR), \theta_s = 2\pi/(1+FR)$.

Fig. 10 shows the contour map for designing the Case III coupler. From the figure, it can be seen that the realizable FR range for Case III is found to be from 6 to 9.4. As an example, for a tight coupling dual-band coupler with a FR of 8, the point P_1 is chosen. The electrical lengths of θ_1, θ_2,

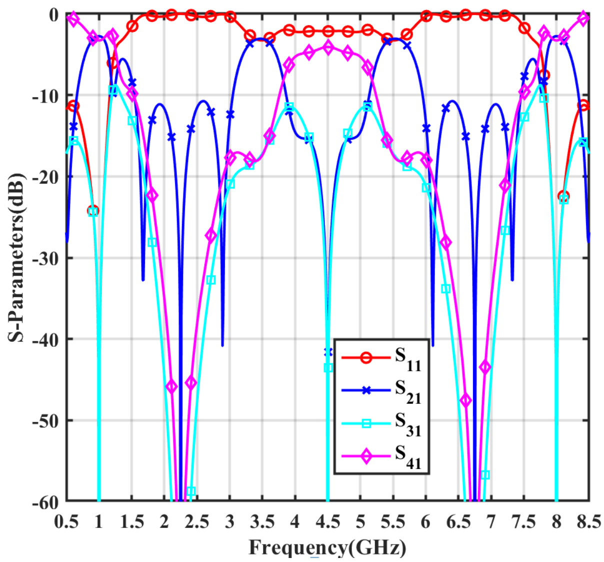

FIGURE 11. Calculated *S*-parameters of the design corresponding to the point P_1 in Fig. 10.

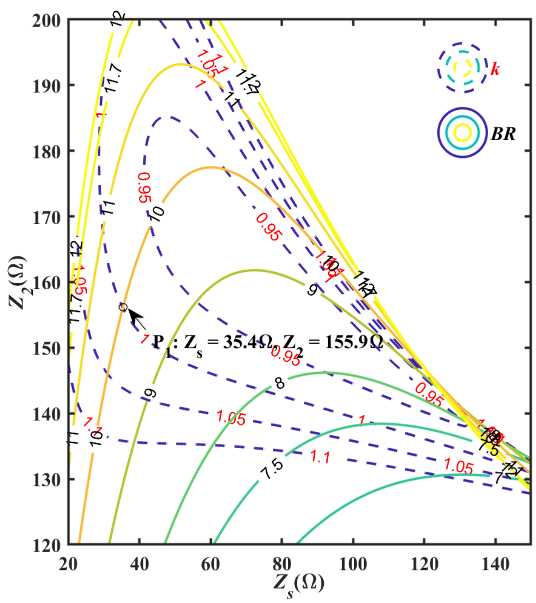

FIGURE 12. Contour map for *k* and *FR* versus Z_s and Z_2 for Case IV.

θ_s can be calculated as 80°, 40°, 10°. Z_e is predetermined to be 80 Ω. Z_s and Z_2 are determined as 35.2 Ω and 142.3 Ω respectively. The calculated *S*-parameters of the design which corresponds to the point P_1 are shown in Fig. 11.

D. Case IV ($\theta_1 = 10\theta_2, \theta_s = 6\theta_2$, FR: 7.5-11.7)

For Case III, $10\theta_2$ and $6\theta_2$ are used to replace θ_1 and θ_s in (7b) and (10). The related parameters of Case III coupler at f_L can be obtain as: $\theta_2 = (\pi/2)/(1+FR)$, $\theta_1 = 5\pi/(1+FR)$, $\theta_s = 3\pi/(1+FR)$.

Fig. 12 shows the contour map for designing the Case III coupler. From the figure, the realizable *FR* range for Case III is found to range from 7.5 to 11.7. As an example, a tight coupling dual-band coupler with a *FR* of 10, the point P_1 is chosen. The electrical lengths of θ_1, θ_2, θ_s can be calculated as 81.82°, 8.18°, 49.09°. Z_e is predetermined to be 80 Ω. Z_s and Z_2 are determined as 35.4 Ω and 155.9 Ω respectively. The calculated *S*-parameters of the design which corresponds to the point P_1 are shown in Fig. 13.

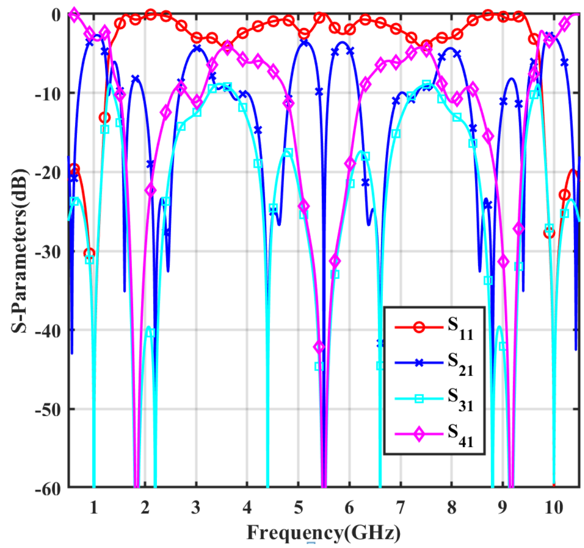

FIGURE 13. Calculated *S*-parameters of the design corresponding to the point P_1 in Fig. 12.

E. Case V ($\theta_1 = 2\theta_2, \theta_s = 2\theta_2$, FR: 1.4-2.8)

For Case IV, $2\theta_2$ and $2\theta_2$ are used to replace θ_1 and θ_s in (7b) and (10). The related parameters of Case IV coupler at f_L can be obtain as: $\theta_2 = (\pi/2)/(1+FR)$, $\theta_1 = \pi/(1+FR)$, $\theta_s = \pi/(1+FR)$.

Fig. 14 shows the contour map for designing the Case IV coupler. It can be seen from the figure that the realizable *FR* range for Case IV is found to range from 1.4 to 2.8. As an example, for a tight coupling dual-band coupler with a *FR* of 2, the point P_1 is chosen in Fig. 14. The electrical lengths of θ_1, θ_2, θ_s can be calculated as 60°, 30°, 60°. Z_e is predetermined to be 86 Ω. Z_s and Z_2 are determined as 67.5 Ω and 48.11 Ω respectively. The calculated *S*-parameters of the design which corresponds to the point P_1 are shown in Fig. 15.

IV. DUAL BAND COUPLER WITH WIDE FREQUENCY RATIO ARBITRARY POWER DIVISION RATIOS OVER TWO BANDS

As stated in the introduction, the characteristics in providing arbitrary power division ratios over two bands is also important for a dual-band coupler. A further investigation on the implementation of arbitrary power division ratios on the proposed structure will be conducted in this section. According to the isolation and matching conditions given in (11a), the four key parameters Z_2, Z_s, θ_2, θ_s are responsible for

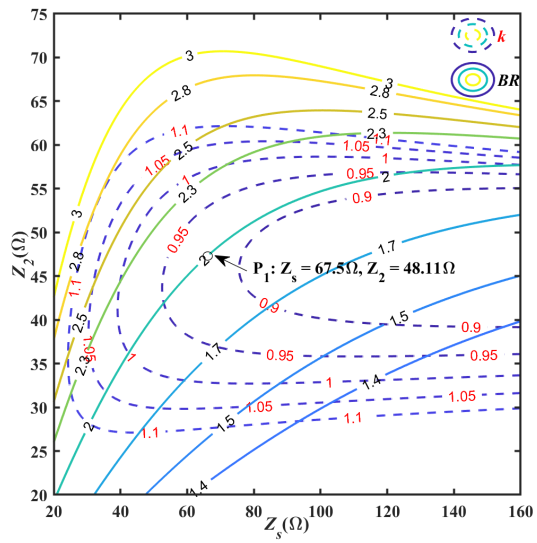

FIGURE 14. Contour map for k and FR versus Z_s and Z_2 for Case V.

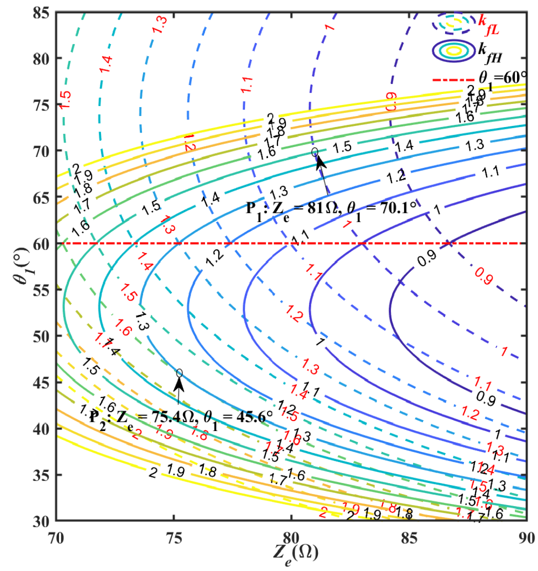

FIGURE 16. Contour map for k_{fL} and k_{fH} versus Z_e and θ_1 with a FR of 2.

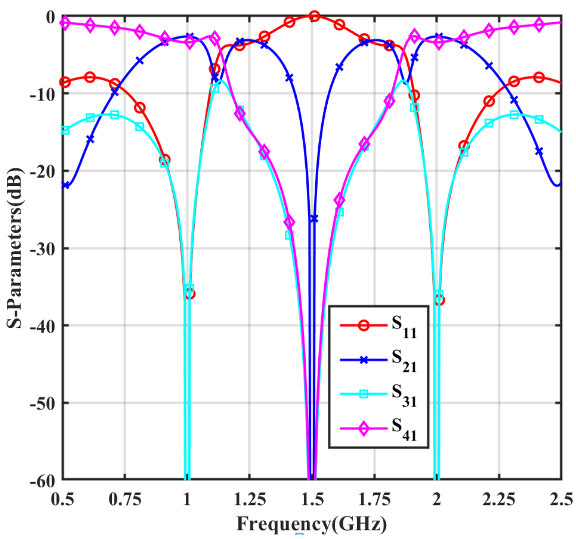

FIGURE 15. Calculated S-parameters of the design corresponding to the point P_1 in Fig. 14.

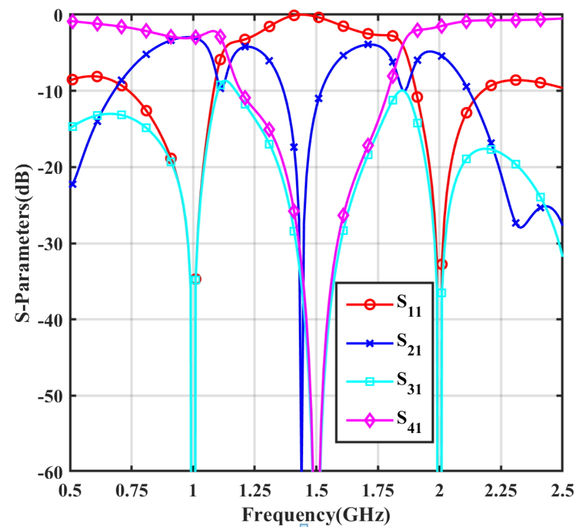

FIGURE 17. Calculated S-parameters of the design corresponding to the point P_1 in Fig. 16.

controlling the frequency ratio. From equation (11b), two additional key parameters Z_e, θ_1 are responsible for controlling the power division ratio k once the frequency ratio is fixed. As Z_e is constant with varying frequency, it will have the same impact on coupling coefficient over the two bands. Therefore, simultaneous arbitrary power ratios for two bands ($k_{fL} = k_{fH}$, k_{fL}, k_{fH} are the power division ratios at f_L and f_H respectively) can be achieved by choosing proper Z_e. However, for different θ_1 at the lower band, it will have different impacts on the power division ratio at both lower and upper band. This is because different electrical lengths of the coupled line at f_L and f_H will lead to different trigonometric functions which correspond different k at two frequency points according to (10). Therefore, different power division ratios can be achieved at two bands ($k_{fL} \neq k_{fH}$) by choosing the proper θ_1 at f_L.

The design procedures for the proposed dual-band coupler can be summarized as follows:

1. According to the desired FR, choose a proper point in the contour map according to the design curves given in Section III.
2. Substitute the chosen Z_s, Z_2, θ_2 and θ_s into (11b), thereafter only three variables θ_1, Z_e and k remain unknown. The contour map for a power division ratio k_{fL} at f_L and k_{fH} at f_H can be plotted.
3. If the same power division ratio is desired for two operating frequencies, the proper value of Z_e can be chosen from the specific line.
4. If different power division ratios are desired for two operating frequencies, a point can be chosen from the

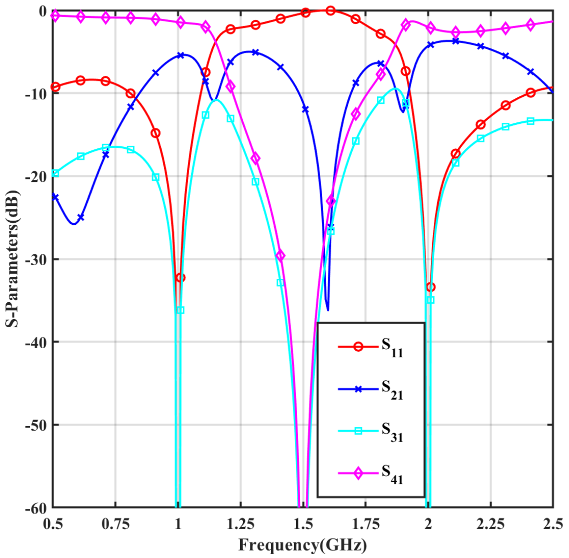

FIGURE 18. Calculated S-parameters of the design corresponding to the point P_2 in Fig. 16.

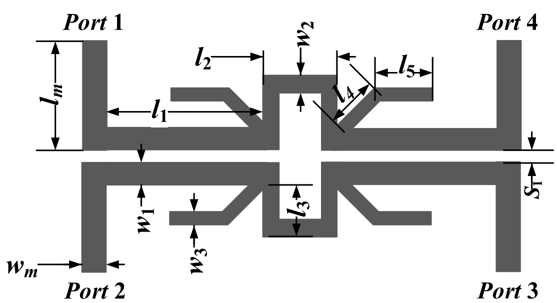

FIGURE 19. The microstrip layout of the proposed dual-band coupler.

contour map according to desired power division ratios at f_L and f_H and then obtain the design parameters θ_1 and Z_e.

A design example with a frequency ratio of 2 based on Case V is used here to illustrate the design procedure. The corresponding Z_s, Z_2, θ_2, and θ_s are 67.5 Ω, 48.11 Ω, 30°, 60° respectively. Fig. 16 shows the design contour map according to the analysis of Case V. θ_s and θ_2 are determined as 60° and 30° at f_L.

From Fig. 16, it can be found that equal power division is been achieved at two frequencies when $\theta_1 = 60°$, k_{fL} and k_{fH} will be the same for different Z_e which is consistent with the analysis above. When θ_1 deviates away from 60°, k_{fL} and k_{fH} will be different for various Z_e, thereby achieving arbitrary power division ratios for f_L and f_H. To design a dual-band coupler with $k_{fL} = 1$ at f_L and $k_{fH} = 1.5$ at f_H, the point P_1 can be chosen from Fig. 16. The calculated S-parameters are shown in Fig. 17. To design a dual-band coupler with $k_{fL} = 1.6$ at f_L and $k_{fH} = 1.3$ at f_H, as an alternative the point P_1 can be chosen. The calculated S-parameters of this design are shown in Fig. 18.

TABLE 1. The detailed dimensional parameters of the two prototypes.

Parameters	Coupler A	Coupler B
l_m	8	7.8
l_1	16.5	44.7
l_2	5.1	2.6
l_3	4.6	4.6
l_4	3.7	3.5
l_5	10.4	20.5
w_m	1.7	1.7
w_1	1.2	1.2
w_2	1.9	0.3
s_1	0.08	0.09

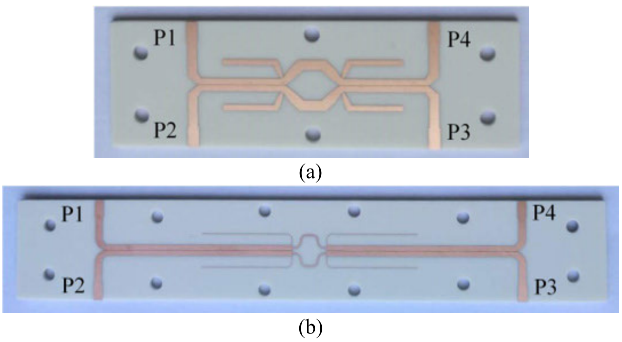

FIGURE 20. The photographs of the fabricated couplers. (a) Coupler A. (b) Coupler B.

V. EXPERIMENTAL VERIFICATION

To verify the proposed theory, a dual-band coupler with equal power division ratio (Coupler A) and a dual-band coupler with different power division ratios at two bands (Coupler B) have been designed, fabricated and measured. For Coupler A, the power-dividing coefficient k is set to be 1 for $f_L = 1$ GHz and $f_H = 6$ GHz. As the desired FR is 6, the Case III structure can be utilized. Thus the detailed values of the design parameters could be obtained from Fig. 8 as: $Z_e = 80\Omega$, $Z_o = 31.25\Omega$, $Z_s = 134.5\Omega$, $Z_2 = 100.1\Omega$, $\theta_1 = 102.86°$, $\theta_s = 51.43°$, $\theta_2 = 12.86°$. For Coupler B, the power-dividing coefficient k is set to be 1 and 1.5 at 2 GHz and 4 GHz respectively. As the coupler has different power division ratios for the two bands, the design theory given in Section IV can be used. Thus the detailed values of the design parameters are obtained from Fig. 16 as: $Z_e = 81\Omega$, $Z_o = 30.86\Omega$, $Z_s = 67.5\Omega$, $Z_2 = 48.11\Omega$, $\theta_1 = 70.1°$, $\theta_s = 60°$, $\theta_2 = 30°$.

These two dual-band couplers are designed based on the substrate Rogers RO4003C with a relative dielectric constant ε_r of 3.38 and a thickness h of 1.524 mm. The microstrip layout of the proposed dual-band coupler is shown in Fig. 19. To consider the junction discontinuity, the commercial electromagnetic full-wave simulation software Ansoft HFSS is used to obtain the optimum designs. The detailed dimensional parameters of the two prototypes are listed in Table I.

TABLE 2. Summarized measured results of the implemented couplers.

Couplers	f (GHz)	$\|S_{11}\|$ (dB)	$\|S_{21}\|$ (dB)	$\|S_{31}\|$ (dB)	$\|S_{41}\|$ (dB)	Phase Difference(°)	BW(%) $\|S_{11}\|$<-10 dB	BW(%)@$f_1\|f_2$ $\|S_{21}\|$ variation	BW(%) $\|S_{31}\|$<-10 dB	BW(%)@$f_1\|f_2$ $\|S_{41}\|$ variation	BW(%) φ@$f_1\|f_2$±5°
A	1	-25.37	-3.59	-24.77	-3.23	-90.94	>84	22.5(±0.5 dB) 32(±1 dB)	>100	28(±0.5 dB) 38(±1 dB)	72
	6	-33.54	-4.31	-18.74	-4.20	-88.02	>18	4.08(±0.5 dB) 5.5(±1 dB)	>100	7.58(±0.5 dB) 10.3(±1 dB)	6
B	2	-14.38	-4.08	-19.31	-3.54	-90.71	>23	13.5(±0.5 dB) 20.5(±1 dB)	>23	21.5(±0.5 dB) 29(±1 dB)	25.5
	4	-12.67	-5.78	-16.32	-3.18	-93.01	16.8	6.38(±0.5 dB) 8.3(±1 dB)	>11.5	4.38(±0.5 dB) 9(±1 dB)	9.5

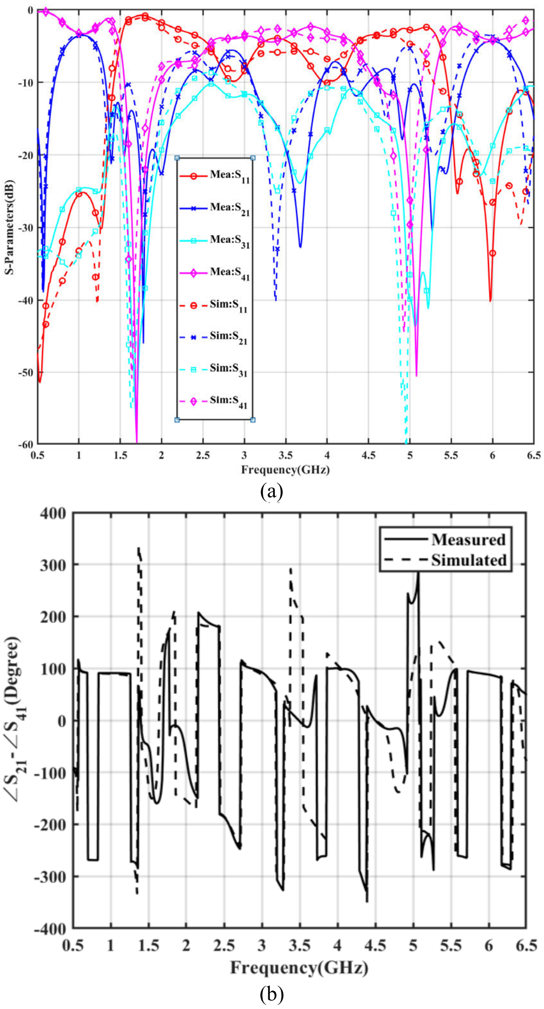

FIGURE 21. Simulated and measured results of the coupler A. (a) *S*-parameters response. (b) Phase difference response.

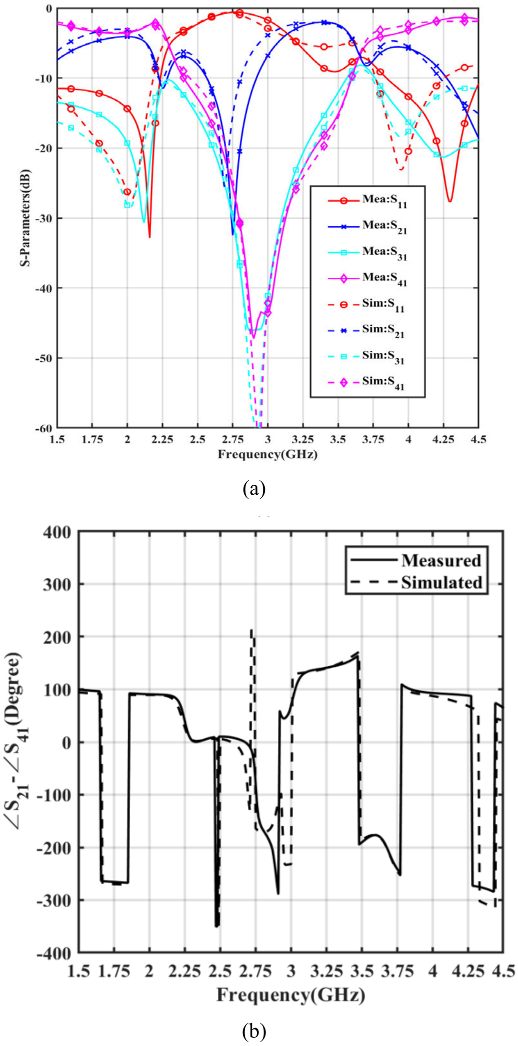

FIGURE 22. Simulated and measured results of the coupler B. (a) *S*-parameters response. (b) Phase difference response.

The photographs of the fabricated prototypes are shown in Fig. 20.

Fig. 21 shows the simulated and measured frequency responses of the implemented coupler A. Good agreement between simulation and measurement can be observed. The discrepancy between simulated and measured results found at 6 GHz is caused by the fabrication error and the losses of the dielectric substrate and connectors. As expected, the quadrature equal power division have been realized simultaneously at 1 GHz and 6 GHz. The detailed performance parameters are summarized in Table II.

Fig. 22 shows the simulated and measured results of coupler B. Similar to the previous design, the measured results also agree well with the simulated ones. This coupler provides coupling coefficients of 3 dB and 6 dB at 2 GHz and 4 GHz

TABLE 3. Comparison between proposed structure and previous works.

	Type	f_H/f_L (GHz)	Coupling (dB)	Transmission (dB)	Phase Difference (°)	BW (%)[1] Coupling Imbalance	FR Range	APD[2]	Tight coupling	Size[3] (λ_L^2)
Coupler A	**Coupled Line**	**1/6 (6)**	**-3.59/-4.31**	**-3.23/-4.20**	**-90.94/-88.0**	**22.5/4.08 (±0.5)**	**1.4-11.7**	**Yes**	**Yes**	**0.654×.0628 (0.0411)**
Coupler B	**Coupled Line**	**2/4 (2)**	**-4.08/-5.78**	**-3.54/-3.18**	**-90.71/-93.0**	**13.5/4.38 (±0.5)**	**1.4-11.7**	**Yes**	**Yes**	**0.595×0.121 (0.0720)**
[14]	Branch Line	2.45/5.2 (2.12)	-4.23/-7.68	-1.07/-0.88	-87.8/-86.9	10.5/15.1 (±0.5)	1.8-2.8	Yes	Yes	0.152×0.124 (0.0188)
[15]	Branch Line	2.4/5.2 (2.17)	9.67/6.71[4]	0.50/1.04[4]	61.91/79.18	7.84/2.92 (±1)	2-3	Yes	Yes	0.5×0.25 (0.1250)
[11]	Patch	3/4.5 (1.5)	11.4/4	1.1/3.9	97.3/90.9	9.3/NA (NA)	1.3-2.2	Yes	Yes	0.35×0.26 (0.0910)
[12]	Coupled Line	2.4/5.8 (2.42)	-9.2/-9.1	-0.7/-1	-90/90	22/19.8 (±1)	2.3-6.7	No	No	1.15×0.02 (0.0230)
[16] Coupler A	Coupled Line	0.84/5.17 (6.15)	-10.6/-10.8	-0.56/-1.32	90.5/-88.5	45/7.4 (±0.5)	<7	No	No	0.33×0.07 (0.0231)
[16] Coupler B	Coupled Line	0.7/2.6 (3.71)	-11.29/-11.13	-0.52/-0.84	90.93/-87.11	24/7 (±0.5)	<10	No	No	0.23×0.11 (0.0253)
[16] Coupler C	Branch Line	0.7/2.55 (3.64)	-3.3/-3.41	-3.46/-3.77	91/-86.7	23.5/8.9 (±0.5)	2-5.4	No	Yes	0.35×0.12 (0.0420)
[17]	Coupled Line	1/5.2 (5.2)	-21.27/-20.9	NA/NA	90/90	121/23.56 (±1)	5-15	No	No	0.81×0.109 (0.0883)

[1] Bandwidth under different coupling imbalance; [2] Arbitrary power division over two bands;
[3] The wavelength is defined at the lower frequency; [4] Calculated using the power division without considering loss.

respectively whilst maintaining quadrature phase characteristics. This verifies the flexibility of the proposed structure in implementing arbitrary power division ratios over two bands. The detailed performance parameters are also summarized in Table II.

To highlight the advantages of the proposed work, a comparison with previous works based on a single element is summarized in Table III. First of all, the proposed work achieves the largest frequency ratio among the works [11], [12], [14], [15] which can provide arbitrary coupling coefficient and also tight coupling up to 3 dB. Moreover, the proposed work also achieves the tightest coupling among the works [16], [17] which can provide the large frequency ratio. Besides, the proposed topology can provide a very wide frequency ratio ranging from 1.4 to 11.7 based on different cases, which cannot be achieved by other existing works. Finally, the proposed work has a simple design procedure, as the related design parameters can be easily obtained using the contour map and equations.

VI. CONCLUSION

In this paper, a novel dual-band coupler topology based on coupled line structure has been proposed. The coupler can provide a wide frequency ratio ranging from 1.4 to 11.7. Within the range, arbitrary power division ratio could be easily achieved for two bands and with a maximum coupling coefficient up to 3 dB. The detailed theory, analysis, and design graphs have been given, making possible the quick design of a dual-band coupler. For demonstration purposes, a 3 dB dual-band coupler with a large frequency ratio of 6 and a dual-band coupler with different power division ratios have been designed, fabricated and measured to verify the newly proposed coupler.

REFERENCES

[1] I.-H. Lin, M. DeVincentis, C. Caloz, and T. Itoh, "Arbitrary dual-band components using composite right/left-handed transmission lines," *IEEE Trans. Microw. Theory Techn.*, vol. 52, no. 4, pp. 1142–1149, Apr. 2004.
[2] K.-K. M. Cheng and F.-L. Wong, "A novel approach to the design and implementation of dual-band compact planar 90° branch-line coupler," *IEEE Trans. Microw. Theory Techn.*, vol. 52, no. 11, pp. 2458–2463, Nov. 2004.
[3] H. Zhang and K. J. Chen, "A stub tapped branch-line coupler for dual-band operations," *IEEE Microw. Wireless Compon. Lett.*, vol. 17, no. 2, pp. 106–108, Feb. 2007.
[4] M.-J. Park, "Dual-band, unequal length branch-line coupler with center-tapped stubs," *IEEE Microw. Wireless Compon. Lett.*, vol. 19, no. 10, pp. 617–619, Oct. 2009.
[5] L. K. Yeung, "A compact dual-band 90° coupler with coupled-line sections," *IEEE Trans. Microw. Theory Techn.*, vol. 59, no. 9, pp. 2227–2232, Sep. 2011.
[6] C.-H. Yu and Y.-H. Pang, "Dual-band unequal-power quadrature branch-line coupler with coupled lines," *IEEE Microw. Wireless Compon. Lett.*, vol. 23, no. 1, pp. 10–12, Jan. 2013.
[7] M.-J. Park and B. Lee, "Dual-band, cross coupled branch line coupler," *IEEE Microw. Wireless Compon. Lett.*, vol. 15, no. 10, pp. 655–657, Oct. 2005.
[8] H. Kim, B. Lee, and M.-J. Park, "Dual-band branch-line coupler with port extensions," *IEEE Trans. Microw. Theory Techn.*, vol. 58, no. 3, pp. 651–655, Mar. 2010.
[9] Y. Wu, S. Y. Zheng, S. W. Leung, Y. Liu, and Q. Xue, "An analytical design method for a novel dual-band unequal coupler with four arbitrary terminated resistances," *IEEE Trans. Ind. Electron.*, vol. 61, no. 10, pp. 5509–5516, Oct. 2014.
[10] S. Y. Zheng, S. H. Yeung, W. S. Chan, K. F. Man, S. H. Leung, and Q. Xue, "Dual-band rectangular patch hybrid coupler," *IEEE Trans. Microw. Theory Techn.*, vol. 56, no. 7, pp. 1721–1728, Jul. 2008.
[11] S. Y. Zheng, Y. Wu, Y. Li, Y. Liu, and Y. Long, "Dual-band hybrid coupler with arbitrary power division ratios over the two bands," *IEEE Trans. Compon., Packag., Manuf. Technol.*, vol. 4, no. 8, pp. 1347–1358, Aug. 2014.

[12] X. Wang, W.-Y. Yin, and K.-L. Wu, "A dual-band coupled-line coupler with an arbitrary coupling coefficient," *IEEE Trans. Microw. Theory Techn.*, vol. 60, no. 4, pp. 945–951, Apr. 2012.

[13] K.-S. Chin, K.-M. Lin, Y.-H. Wei, T.-H. Tseng, and Y.-J. Yang, "Compact dual-band branch-line and rat-race couplers with stepped-impedance-stub lines," *IEEE Trans. Microw. Theory Techn.*, vol. 58, no. 5, pp. 1213–1221, May 2010.

[14] C.-L. Hsu, J.-T. Kuo, and C.-W. Chang, "Miniaturized dual-band hybrid couplers with arbitrary power division ratios," *IEEE Trans. Microw. Theory Techn.*, vol. 57, no. 1, pp. 149–156, Jan. 2009.

[15] P.-L. Chi and K.-L. Ho, "Design of dual-band coupler with arbitrary power division ratios and phase differences," *IEEE Trans. Microw. Theory Techn.*, vol. 62, no. 12, pp. 2965–2974, Dec. 2014.

[16] C.-C. Chang, K.-S. Chin, and Y.-C. Chiang, "Dual-band coupled-line couplers with wide separation between bands," *IEEE Trans. Microw. Theory Techn.*, vol. 65, no. 8, pp. 2918–2929, Aug. 2017.

[17] Y. Liu, S. Jiang, S. Zhu, Y. Tian, and Y. Wu, "Large frequency-ratio dual-band and broad dual-band parallel-line couplers," *IEEE Trans. Compon., Packag., Manuf. Technol.*, vol. 8, no. 1, pp. 121–131, Jan. 2018.

[18] X. F. Ye, S. Y. Zheng, Y. M. Pan, D. Ho, and Y. L. Long, "A new class of components for simultaneous power splitting over microwave and millimeter-wave frequency bands," *IEEE Access*, vol. 6, pp. 146–158, 2018.

LIANG GAO was born in Jiangxi, China. He received the B.Eng. degree in electronic information science and technology from Sun Yat-sen University, Guangzhou, China, in 2018. He is currently pursuing the Ph.D. degree with the City University of Hong Kong (CityU), Hong Kong. His current research interests include terahertz radiator and terahertz phased array design using CMOS technology.

SHAO YONG ZHENG (S'07–M'11–SM'17) was born in Fujian, China. He received the B.S. degree in electronic engineering from Xiamen University, Fujian, China, in 2003, and the M.Sc., M.Phil., and Ph.D. degrees in electronic engineering from the City University of Hong Kong, Hong Kong, in 2006, 2008, and 2011, respectively.

From 2011 to 2012, he was a Research Fellow with the Department of Electronic Engineering, City University of Hong Kong, where he was also a Visiting Assistant Professor with the Department of Electronic Engineering, from July 2013 to August 2013, from July 2014 to August 2014, and from July 2015 to August 2015. He is currently an Associate Professor with the School of Electronics and Information Technology, Sun Yat-sen University, Guangzhou, China, and the Deputy Director of the Mobile Communication National Engineering Research Center, SYSU Branch. His research interests include microwave/millimeter wave components and evolutionary algorithms.

WONBIN HONG (S'04–M'09–SM'14) received the B.S. degree in electrical engineering from Purdue University, West Lafayette, IN, USA, in 2004, and the master's and Ph.D. degrees in electrical engineering from the University of Michigan, Ann Arbor, MI, USA, in 2005 and 2009, respectively.

From 2009 to 2016, he was with Samsung Electronics, as the Principal and a Senior Engineer participating and leading extensive Research and Development tasks for upcoming wireless applications, including MIMO, wireless power transfer, and millimeter-wave wireless solutions. He is currently with the Department of Electrical Engineering, Pohang University of Science and Technology (POSTECH), Pohang, South Korea, as an Associate Professor. He has well more than 16 years of extensive research and development experience with primary interest in future wireless communication antennas and RF circuits, mesoscale and nanoscale transparent electronics, and 3D packaging. He has authored or coauthored more than 80 peer-reviewed journals, conference papers, and two book chapters. He is also the inventor of more than 100 patent inventions. He was one of the first to devise the engineering concept of millimeter-wave antennas for 5G mobile terminals. In addition, his patented inventions on optically invisible antennas, which can be integrated within LCD /OLED panels has led to more than four million commercialized productions, since 2016.

Dr. Hong is a member of the Technical Committee of the IEEE MTT-14 Microwave and Millimeter-wave Integrated Circuits, a Technical Committee Member for the IEEE AP-S Industry Initiative Committee (IIC), and the Technical Committee on Antenna Measurements (T-CAM). He has also served in numerous international symposiums and workshops, as a Technical Committee Member and the Session Chair. He and his students have received numerous awards and recognitions for these achievements. He has served as an Invited Lecturer and a Speaker in more than 80 international research symposiums, government, and industry sessions held around the world. From 2016 to 2017, he served as a Guest Editor of the IEEE Transactions on Antennas and Propagation Special Edition on Antennas and Propagation Aspects of 5G Communications. He is currently serving as an Associate Editor of the IEEE Transactions on Antennas and Propagation and the *IEEE Antennas and Propagation Magazine*. He is also a Lead Guest Editor of the IEEE Antennas and Wireless Propagation Letters, Special Cluster on Antenna-in-Package, Antenna-on-Chip, Antenna-IC Interface: Joint Design and Co-integration. He has been involved in more than 25 governments, industry research projects. He is also serves as a Technical Consultant to numerous multinational tech firms, such as Samsung Electronics, LG Electronics, SK Telecom, Corning, Sumitomo, and several other leaders in industry and government agencies.

YUANXIN LI (M'08) was born in Guangzhou, China. He received the B.S. and Ph.D. degrees from Sun Yat-sen University, China, in 2001 and 2006, respectively.

From 2006 to 2008, he was a Senior Research Assistant with the State Key Laboratory of Millimeter Waves, City University of Hong Kong, where he was a Research Fellow, in 2010. Since 2008, he has been with the Department of Electronics and Communication Engineering, Sun Yat-sen University, where he is currently an Associate Professor. His current research interests include microstrip leaky wave antenna and applications of the periodic construction.